

Exact Artificial Boundary Condition for the Poisson Equation in the Simulation of the 2D Schrödinger-Poisson System

Norbert J. Mauser¹ and Yong Zhang^{1,*}

¹ Wolfgang Pauli Institute c/o Fak. Mathematik, University Wien,
Oskar-Morgenstern-Platz 1, 1090 Vienna, Austria.

Received 11 August 2013; Accepted (in revised version) 14 March 2014

Communicated by Ming-Chih Lai

Available online 4 July 2014

Abstract. We study the computation of ground states and time dependent solutions of the Schrödinger-Poisson system (SPS) on a bounded domain in 2D (i.e. in two space dimensions). On a disc-shaped domain, we derive exact artificial boundary conditions for the Poisson potential based on truncated Fourier series expansion in θ , and propose a second order finite difference scheme to solve the r -variable ODEs of the Fourier coefficients. The Poisson potential can be solved within $\mathcal{O}(MN \log N)$ arithmetic operations where M, N are the number of grid points in r -direction and the Fourier bases. Combined with the Poisson solver, a backward Euler and a semi-implicit/leap-frog method are proposed to compute the ground state and dynamics respectively. Numerical results are shown to confirm the accuracy and efficiency. Also we make it clear that backward Euler sine pseudospectral (BESP) method in [33] can not be applied to 2D SPS simulation.

AMS subject classifications: 35Q55, 65M06, 65M22, 65T50, 81-08

Key words: 2D Schrödinger-Poisson system, exact artificial boundary condition, backward Euler scheme, semi-implicit/leap-frog scheme, backward Euler sine pseudospectral method.

1 Introduction

The Schrödinger-Poisson system (SPS) is used, e.g., in quantum semiconductor modelling [2, 20]. We shall deal with the 2D (two space dimensions) case [1]. The system

*Corresponding author. *Email addresses:* `norbert.mauser@univie.ac.at` (N. J. Mauser), `yong.zhang@univie.ac.at` (Y. Zhang)

reads, in rescaled form, as

$$i\partial_t\psi(\mathbf{x},t) = \left(-\frac{1}{2}\Delta + V(\mathbf{x}) + \beta\varphi\right)\psi(\mathbf{x},t), \quad \mathbf{x} \in \mathbb{R}^2, \quad t > 0, \tag{1.1}$$

$$\psi(\mathbf{x},t=0) = \psi_0(\mathbf{x}), \quad \mathbf{x} \in \mathbb{R}^2, \tag{1.2}$$

$$-\Delta\varphi(\mathbf{x},t) = |\psi(\mathbf{x},t)|^2, \quad \mathbf{x} \in \mathbb{R}^2, \quad t > 0, \tag{1.3}$$

where the complex-valued function $\psi(\mathbf{x},t)$ stands for the wave function and decays to zero at far field, i.e., $\lim_{|\mathbf{x}| \rightarrow +\infty} |\psi(\mathbf{x},t)| = 0, \forall t > 0$, ψ_0 is the initial data lying in the energy space $H^1(\mathbb{R}^2)$, $V(\mathbf{x})$ is an external potential and $\beta \in \mathbb{R}$ is a coupling constant that represents the relative strength of the Poisson potential for repulsive case ($\beta > 0$) and attractive case ($\beta < 0$). Note that the Poisson equation (1.3) can be rewritten as a convolution of the density and the Green's function of Laplace operator as follows

$$\varphi(\mathbf{x},t) = \left(-\frac{1}{2\pi}\ln|\mathbf{x}|\right) * |\psi(\mathbf{x},t)|^2. \tag{1.4}$$

Two important invariants are the mass $M(\psi) := \int_{\mathbb{R}^2} |\psi|^2 dx$ and the total energy $E(\psi) := \int_{\mathbb{R}^2} \frac{1}{2} |\nabla\psi|^2 + V(\mathbf{x})|\psi|^2 + \frac{1}{2} \beta\varphi|\psi|^2 dx$. The ground state ϕ_g is defined as the minimizer of the energy E on the unit sphere $S = \{\phi \mid \|\phi\|_{R^2(\mathbb{R}^2)} = 1, E(\phi) < \infty\}$, i.e.,

$$\phi_g = \arg \min_{\phi \in S} E(\phi) \tag{1.5}$$

and the ground state energy is denoted as $E^g = E(\phi_g)$.

The SPS is a "weakly" nonlinear Schrödinger equation (NLS) that has been extensively studied analytically and numerically. For a derivation of the Schrödinger-Poisson system from the linear N-body Schrödinger equation with Coulomb interaction, see e.g. [13,14,18]. For a discussion of the dimension reduction from 3D to 2D for the Schrödinger-Poisson system, see e.g. [10,15].

Here we focus on the numerical aspect of reducing the whole space problem to a numerically tractable problem on a bounded domain, with emphasis on the boundary conditions imposed on the Poisson equation.

Several efficient and accurate numerical methods had been proposed to solve SPS, such as the time-splitting spectral/pseudospectral method [11], finite difference method and finite element method [30]. Particularly, for SPS, we refer the reader to [12,17,33] for the time splitting pseudospectral method, to [26,31] for difference method and etc.

For numerical simulations of Schrödinger type equations, the whole space problem is usually truncated on a bounded domain, assuming that the wave function outside the computation domain is negligible. The easiest way is to truncate the wave function on a bounded domain and to use homogeneous Dirichlet boundary conditions (corresponding to reflection due to an infinite potential) or periodic boundary conditions (called "Born-von Karman boundary conditions" in solid state physics) for the wave function and its gradient.

For the numerical simulation of the non-local Poisson potential in an integral equation version (1.4), we do not need boundary conditions. Convolution-integral based Poisson solvers, such as Fast Multipole Methods [19,23] and Wavelet-based solvers [22], are direct and do not require truncation of whole space, but they are not easy to implement and we shall not consider them in this work.

We deal with the differential equation version (1.3), which is posed on a bounded domain in 2D, either a rectangle or a disc, with appropriate boundary conditions. For example, the plane wave methods, which includes the Fourier/sine pseudo-spectral method, are simple and spectrally accurate on rectangular domains. In 1D and 3D, the SPS was simulated accurately and efficiently by pseudo-spectral method in [17, 33]. However, straightforward extension of these methods using a rectangular domain does not work for the 2D SPS as we shall show in this work.

In 2D, problems with the boundary conditions for Poisson potential arise: if the Poisson potential is enforced periodic boundary conditions on a rectangular domain, Fourier pseudo-spectral discretization of the Poisson equation would encounter similar inconsistency phenomenon as addressed in [33]. At first sight, homogenous Dirichlet boundary condition seems to be applicable, eventually for the price of a large computation domain so as to obtain acceptable accuracy. However, this is not the case: one can prove that the 2D Poisson potential decays logarithmically at far-field (see appendix) and it is not constant-valued on the rectangle boundaries. Hence the simple homogeneous Dirichlet boundary condition does not leave the Poisson potential radial-symmetric in a radial-symmetric setting, and the simulation fails qualitatively. Errors coming from the boundary condition will then dominate even for larger computation domain or smaller mesh size. Non-zero Dirichlet boundary condition is possible, but one still has to solve a Laplace equation with Dirichlet boundary condition on a rectangle, which is not easier either. Thus, it is necessary to use a disc-shaped domain instead of a rectangle and to design accurate boundary conditions for the 2D Poisson equation.

This problem of an accurate and efficient evaluation of 2D Poisson potential has been treated in [16, 21, 27–29] for the case of polar coordinates with different kinds of approximate boundary conditions. For our situation of the 2D SPS, mass is conserved and the wave function that yields the density decays sufficiently fast at far field, and it is possible to derive some exact artificial boundary conditions for the Poisson potential, which can help convert the whole space problem equivalently to a bounded domain problem [9, 24, 25].

In this article, based on truncated Fourier series expansion, we derive exact boundary conditions for the differential equations of the Fourier coefficients and then solve the ODEs by a second order finite different method [27, 28]. The Poisson solver proves to be spectrally accurate in θ -direction and second order accurate in r -direction. Coupled with a backward Euler and a semi-implicit/leap-frog scheme, we compute the ground state and the dynamics of the 2D SPS. Extensive numerical results show that our methods are indeed accurate and efficient.

2 Exact artificial boundary condition for the Poisson equation

As stated before, we truncate the 2D whole space problem to a bounded disc domain $\Omega_R = \{\mathbf{x} \in \mathbb{R}^2 : |\mathbf{x}| \leq R, R > 0\}$ and we use polar coordinates (r, θ) . In this section, we shall derive exact artificial boundary conditions for differential equations for the Fourier coefficients and propose a second-order finite difference scheme to solve the Poisson equation.

2.1 Derivation of artificial boundary conditions

For the SPS system, we can reasonably assume that the wave function and hence the density that enters the Poisson equation as source data decay fast enough. By taking initial data with compact support, we can choose a sufficiently large radius R such that the density $\rho := |\psi|^2$ is compactly supported in Ω_R , i.e.,

$$\text{supp}\{\rho(r, \theta)\} \subset \Omega_R.$$

The density ρ can be approximated by ρ_R that is defined as follows

$$\rho_R(r, \theta) = \begin{cases} |\psi|^2, & 0 \leq r \leq R, \\ 0, & R \leq r < \infty. \end{cases}$$

Thus the Poisson potential φ_R satisfies the following equation

$$-\Delta \varphi_R = |\psi|^2, \quad \mathbf{x} \in \Omega_R, \tag{2.1}$$

$$-\Delta \varphi_R = 0, \quad \mathbf{x} \in \Omega_R^c, \tag{2.2}$$

where the Laplacian in polar coordinates: $\Delta = \frac{1}{r} \frac{\partial}{\partial r} (r \frac{\partial}{\partial r}) + \frac{1}{r^2} \frac{\partial^2}{\partial \theta^2}$.

For simplified notation, we drop the index R and write again φ and ρ for φ_R, ρ_R , respectively. Since φ and ρ are periodic in θ , they both can be approximated by finite Fourier series as

$$\varphi(r, \theta) = \sum_{k=-N/2}^{N/2-1} \varphi_k(r) e^{ik\theta}, \quad \rho(r, \theta) = \sum_{k=-N/2}^{N/2-1} \rho_k(r) e^{ik\theta}, \quad 0 \leq r < \infty, \tag{2.3}$$

where N is an even positive number and the coefficients $\varphi_k(r), \rho_k(r)$ are defined as

$$\varphi_k(r) = \frac{1}{2\pi} \int_0^{2\pi} \varphi(r, \theta) e^{-ik\theta} d\theta, \quad \rho_k(r) = \frac{1}{2\pi} \int_0^{2\pi} \rho(r, \theta) e^{-ik\theta} d\theta. \tag{2.4}$$

Plugging (2.3) into the exterior problem (2.2), we obtain

$$\partial_r^2 \varphi_k + \frac{1}{r} \partial_r \varphi_k - \frac{k^2}{r^2} \varphi_k = 0, \quad R \leq r < \infty \tag{2.5}$$

for any $k = -N/2, \dots, N/2 - 1$. Eq. (2.5) can be solved analytically.

For $k \neq 0$, we have $\varphi_k(r) = Cr^{\pm|k|}$. We just take $\varphi_k(r) = Cr^{-|k|}$ here because the Poisson potential does not grow polynomially fast at far field. By a simple calculation, we can derive Robin boundary condition as follows

$$\partial_r \varphi_k|_{r=R} = -\frac{|k|}{r} \varphi_k|_{r=R}. \quad (2.6)$$

For $k = 0$, we have $\varphi_0(r) = a \ln(r) + b$. The transversal property of NLS allows for a constant shift of $\varphi_0(r)$ without affecting the density evolution, thus $\varphi_0(r)$ can be shifted as $a \ln(r)$. In fact, it can be proved rigorously that $b = 0$ (see appendix). Similarly, we have

$$\partial_r \varphi_0|_{r=R} = \frac{\varphi_0}{r \ln(r)}|_{r=R}. \quad (2.7)$$

Up to now, we have derived exact artificial boundary conditions for the Fourier coefficients φ_k . Plugging (2.3) into (2.1), we have for $k = -N/2, \dots, N/2 - 1$

$$\partial_r^2 \varphi_k + \frac{1}{r} \partial_r \varphi_k - \frac{k^2}{r^2} \varphi_k = -\rho_k, \quad 0 \leq r \leq R, \quad (2.8)$$

with the "exact artificial boundary conditions"

$$\partial_r \varphi_0(R) = \frac{\varphi_0(R)}{R \ln(R)}, \quad \text{and} \quad \partial_r \varphi_k(R) = -\frac{|k|}{R} \varphi_k(R), \quad k \neq 0. \quad (2.9)$$

By standard variational methods and a maximal principle it can be proven that Eq. (2.8) with the boundary conditions (2.9) admits unique solutions. Since the Poisson potential φ and the source term ρ are both well-defined continuous functions, they satisfy pole conditions [21, 29] as follows

$$\partial_r \varphi_0(0) = 0, \quad \varphi_k(0) = 0, \quad k \neq 0. \quad (2.10)$$

We remark that it is not necessary to treat (2.10) as boundary conditions, the solution to (2.8)-(2.9) satisfies (2.10) automatically in SPS.

2.2 Numerical scheme to solve the Poisson equation

In this subsection, we propose a numerical method to solve the boundary value problem (2.8)-(2.9). First, Eqs. (2.8)-(2.9) are discretized by second order finite difference method on a uniform mesh with a half grid shift as proposed by M.-C. Lai et al. [27, 28]. For the Robin boundary problem, we choose an integer $M > 0$, a mesh size $\Delta r = R/M$ and grid point $r_j = (j - 1/2)\Delta r$, $j = 0, 1, \dots, M+1$ with $r_M = R - \frac{1}{2}\Delta r$, $r_{M+1} = R + \frac{1}{2}\Delta r$. Let $\varphi_{k,j}$, $\rho_{k,j}$ be the approximation of $\varphi_k(r_j)$, $\rho_k(r_j)$ respectively. Then Eq. (2.8) is discretized as

$$\frac{\varphi_{k,j+1} - 2\varphi_{k,j} + \varphi_{k,j-1}}{(\Delta r)^2} + \frac{1}{r_j} \frac{\varphi_{k,j+1} - \varphi_{k,j-1}}{2\Delta r} - \frac{k^2}{r_j^2} \varphi_{k,j} = -\rho_{k,j}, \quad j = 1, \dots, M, \quad (2.11)$$

for $k = -N/2, \dots, N/2 - 1$. The Robin boundary conditions are approximated as

$$\frac{\varphi_{0,M+1} - \varphi_{0,M}}{\Delta r} = \frac{\varphi_{0,M+1} + \varphi_{0,M}}{2R \ln R}, \tag{2.12}$$

$$\frac{\varphi_{k,M+1} - \varphi_{k,M}}{\Delta r} = -\frac{\varphi_{k,M+1} + \varphi_{k,M}}{2} \frac{|k|}{R}, \quad k \neq 0. \tag{2.13}$$

Notice that $\varphi_{k,M+1}$ can be expressed in terms of $\varphi_{k,M}$ via (2.12)-(2.13) and the coefficient of $\varphi_{k,0}$ equals to $\frac{1}{(\Delta r)^2} - \frac{1}{2r_1 \Delta r} = 0$, thus we can solve the tridiagonal linear system with $\mathcal{O}(M)$ arithmetic operations for each k . The Fourier coefficient in (2.4) can be approximated by applying a trapezoidal rule and it can be accelerated by discrete Fast Fourier Transform (FFT) within $\mathcal{O}(MN \log N)$ arithmetic operations.

Since the Poisson equation has to be solved several times, efficiency is of great importance. The coefficients of the N resultant tridiagonal linear systems keep unchanged, thus we only need to compute them once. The total memory cost of the linear systems is $\mathcal{O}(MN)$. The overall computational cost for a given source term $\rho(r_j, \theta_k)$, which consists of transformation between physical and phase space via Fast Fourier Transform (FFT) and N tridiagonal linear systems, is $\mathcal{O}(MN \log N)$.

Remark 2.1. As stated in [27,28], higher order finite difference discretization of the boundary value problems is possible if the Robin boundary conditions are dealt with properly. Apart from the finite difference method we present, one could also apply finite element method as introduced in [8]. Also there are many papers interested in spectral/pseudospectral collocation/Galerkin method to solve Poisson equation in polar geometry [16, 29], however, to the authors' knowledge, no such method combined with artificial boundary condition has ever been proposed for (2.8)-(2.9). It is interesting and also promising if spectral method is combined with artificial boundary condition.

Remark 2.2. The artificial boundary condition method can be extended to 3D SPS, where the wave function and the Poisson potential are expanded by spherical harmonics, i.e., $Y_l^m(\theta, \phi)$. By solving a similar exterior Laplace equation, we can derive exact artificial boundary conditions for the Fourier coefficients of the Poisson potential. The reduced 1D differential equation together with exact artificial boundary conditions can be solved similarly by finite different method. Research work on extension to 3D SPS is still ongoing.

3 Numerical methods to compute SPS

In this section, we present numerical methods to compute the ground state and dynamics of SPS based on exact artificial boundary conditions for the Poisson equation. Introduce a mesh grid $(r_j, \theta_l), j = 0, \dots, M+1, l = 0, \dots, N-1$ where r_j is the same as specified in the last section and $\theta_l = l \Delta \theta, l = 0, \dots, N-1$ with $\Delta \theta = \frac{2\pi}{N}$. Denote the time by $t_n = n\tau, n = 0, 1, \dots$ with τ being the time step.

3.1 Numerical method for computing the ground state

For computing the ground states of 2D SPS, we adapt the gradient flow with discrete normalization (GFDN) [7] which has been widely and successfully used for computing ground states of the Gross-Pitaevskii equation (GPE) with application to Bose-Einstein condensation (BEC) [3, 5]. We refer to [3, 7, 33] for detailed description of GFDN.

The gradient flow with discrete normalisation (GFDN) for (1.5) reads as follows

$$\phi_t = \frac{1}{2} \Delta \phi - V \phi - \beta \phi |\phi|^2, \quad t_n < t < t_{n+1}, \quad (3.1)$$

$$\phi = -\frac{1}{2\pi} \ln(|\mathbf{x}|) * |\phi|^2, \quad \lim_{r \rightarrow \infty} \phi(r, \theta, t) = 0, \quad t > 0, \quad (3.2)$$

$$\phi(\cdot, t_{n+1}) = \frac{\phi(\cdot, t_{n+1}^-)}{\|\phi(\cdot, t_{n+1}^-)\|}, \quad n \geq 1, \quad (3.3)$$

$$\phi(r, \theta, 0) = \phi_0(r, \theta) \geq 0, \quad 0 \leq r < \infty, \quad 0 \leq \theta \leq 2\pi, \quad (3.4)$$

where $\|\phi_0\| = 1$ and the norm $\|\cdot\|$ is defined as

$$\|\phi\|^2 = \int_0^\infty r \, dr \int_0^{2\pi} |\phi(r, \theta)|^2 \, d\theta. \quad (3.5)$$

Numerically, let $\phi_{jl}^n, \varphi_{jl}^n, V_{jl}$ be approximation of $\phi(r_j, \theta_k, t_n), \varphi(r_j, \theta_k, t_n), V(r_j, \theta_k)$ on Ω_R . A backward Euler finite difference discretization (**BEFD**) reads as

$$\frac{\phi_{jl}^* - \phi_{jl}^n}{\tau} = \frac{1}{2} \Delta \phi_{jl}^* - \beta \varphi_{jl}^n \phi_{jl}^* - V_{jl} \phi_{jl}^*, \quad (3.6)$$

$$\phi_{jl}^{n+1} = \frac{\phi_{jl}^*}{\|\phi^*\|}, \quad n = 1, 2, \dots, \quad (3.7)$$

$$\phi_{jl}^0 = \phi_0(r_j, \theta_l), \quad j = 1, \dots, M, \quad l = 0, \dots, N-1, \quad (3.8)$$

where φ_{jl}^n is determined by (2.11)-(2.13) with source term $|\phi_{jl}^n|^2$ and the discrete norm $\|\phi^*\|$ is approximated as $\|\phi^*\| = \sqrt{\sum_{j=1}^{M-1} \sum_{l=0}^{N-1} |\phi_{jl}^*|^2 r_j \Delta r \Delta \theta}$. The nonlinear equation (3.6) can be solved iteratively [6, 32] as

$$\frac{\phi_{jl}^{*,s+1} - \phi_{jl}^n}{\tau} = \frac{1}{2} \Delta \phi_{jl}^{*,s+1} - \beta \varphi_{jl}^n \phi_{jl}^{*,s} - V_{jl} \phi_{jl}^{*,s} \quad (3.9)$$

with $\phi_{jl}^{*,0}$ being some simple approximation of ϕ_{jl}^* . Note that to compute $\Delta \phi$, one can first expand ϕ into Fourier series and then discretize $\Delta \phi$ by a central finite difference scheme in r -direction as follows

$$\begin{aligned} \Delta \phi \Big|_{(r_j, \theta_l)} &\approx \sum_{k=-N/2}^{N/2-1} \left(\partial_{rr} + \frac{1}{r} \partial_r - \frac{k^2}{r^2} \right) \phi_k e^{ik\theta_l} \Big|_{(r_j, \theta_l)} \\ &= \sum_{k=-N/2}^{N/2-1} \left[\frac{\varphi_{k,j+1} - 2\varphi_{k,j} + \varphi_{k,j-1}}{(\Delta r)^2} + \frac{1}{r_j} \frac{\varphi_{k,j+1} - \varphi_{k,j-1}}{2\Delta r} - \frac{k^2}{r_j^2} \varphi_{k,j} \right] e^{ik\theta_l}. \end{aligned}$$

Remark 3.1. If the external potential $V(r, \theta) = V(r)$ is radial symmetric, the ground state ϕ and Poisson potential φ are also radial symmetric and the 2D SPS would be reduced to a 1D problem.

3.2 Numerical method for computing the dynamics

In this subsection, we discretize the SPS in θ -direction by Fourier pseudospectral method, in r -direction by finite difference method and in time by a semi-implicit/leap-frog scheme on Ω_R with Dirichlet boundary condition $\psi(R, \theta, t) = 0$.

Let $\psi^n, \varphi^n, \psi_k^n$ denote $\psi(r, \theta, t_n), \varphi(r, \theta, t_n), \psi_k^n(r)$ and $\psi_{k,j}^n, \psi_{j,k}^n$ be the numerical approximations of the Fourier coefficients $\psi_k(r_j, t_n)$ and the wave function $\psi(r_j, \theta_k, t_n)$ respectively.

The SPS is discretized by semi-implicit/leap-frog finite difference method (SIFD) as [4, 32]

$$i \frac{\psi^{n+1} - \psi^{n-1}}{2\tau} = -\frac{1}{2} \Delta \left(\frac{\psi^{n+1} + \psi^{n-1}}{2} \right) + V(r, \theta) \psi^n + \beta \varphi^n \psi^n, \quad n \geq 1, \quad (3.10)$$

where the Poisson potential φ^n are determined by (2.11)-(2.13) with source term $|\psi^n|^2$.

The first step value ψ^1 is computed by a second order modified Euler method as

$$\psi^1 = \psi^0 - i \tau \left[-\frac{1}{2} \Delta \psi^{(1)} + V(r, \theta) \psi^{(1)} + \beta \varphi^{(1)} \psi^{(1)} \right], \quad (3.11)$$

$$\psi^{(1)} = \psi^0 - i \frac{\tau}{2} \left[-\frac{1}{2} \Delta \psi^0 + V(r, \theta) \psi^0 + \beta \varphi^0 \psi^0 \right], \quad (3.12)$$

where $\varphi^{(1)}$ are computed by (2.11)-(2.13) with source term $|\psi^{(1)}|^2$.

Expanding both sides of (3.10) by Fourier series, Eq. (3.10) is rewritten, in Fourier space, as

$$i \frac{\psi_k^{n+1} - \psi_k^{n-1}}{2\tau} = -\frac{1}{2} \left(\partial_r^2 + \frac{1}{r} \partial_r - \frac{k^2}{r^2} \right) \left(\frac{\psi_k^{n+1} + \psi_k^{n-1}}{2} \right) + (V \psi^n + \beta \varphi^n \psi^n)_k, \quad n \geq 1, \quad (3.13)$$

subject to homogeneous Dirichlet boundary condition

$$\psi_k^{n-1}(R) = \psi_k^n(R) = \psi_k^{n+1}(R) = 0, \quad (3.14)$$

where $\psi_k^n = \psi_k(r, t_n)$ and $(V \psi^n + \beta \varphi^n \psi^n)_k$ is the k -th Fourier coefficient of $V \psi^n + \beta \varphi^n \psi^n$. If $V(r, \theta) = V(r)$, we can incorporate $V(r)$ into the implicit part, then we have

$$i \frac{\psi_k^{n+1} - \psi_k^{n-1}}{2\tau} = -\frac{1}{2} \left(\partial_r^2 + \frac{1}{r} \partial_r - \frac{k^2}{r^2} + V(r) \right) \left(\frac{\psi_k^{n+1} + \psi_k^{n-1}}{2} \right) + (\beta \varphi^n \psi^n)_k, \quad n \geq 1. \quad (3.15)$$

Applying a central finite difference method to (3.13)/(3.15) and (3.14) on grid points $r_j, j=1, \dots, M$, the resulting linear system is tridiagonal and it can be solved within $\mathcal{O}(M)$ operations for each k . Then the wave function ψ_{jk}^{n+1} can be obtained via FFT from $\psi_{k,j}^{n+1}$. The computation of $\psi^1, \psi^{(1)}$ are explicit and the Laplacian of $\psi^{(1)}, \psi^0$ therein could be calculated similarly.

Remark 3.2. If the initial wave function ψ_0 and external potential V are both radial symmetric, the 2D SPS can be reduced to 1D problem which could be processed similarly as in Subsection 3.1.

4 Numerical results

Based on the numerical methods we proposed in Section 3, in this section, extensive numerical results for computing the ground state and dynamics of 2D SPS under different setups are reported.

4.1 Numerical results in computation of ground state

In this subsection, we present numerical results in computation of ground state together with some comparison with 2D backward Euler sine pseudospectral method (**BESP**) introduced on rectangular domain.

Accuracy. To test the accuracy of BEFD for the ground state, we choose the attractive interaction case, i.e., $\beta < 0$ without external potential. Then the ground state is radial symmetric and the 2D BEFD is reduced to 1D. The initial guess for ground state is set as $\phi_0 = \sqrt{2/\pi} e^{-r^2}$. The numerical 'exact' solution ϕ_g^e is obtained with a fine mesh $\Delta r = 1/256$. Let $\phi_g^{\Delta r}$ denote the numerical solution computed with mesh Δr and $R = 16$. Table 1 shows the discrete maximal errors $\|\phi_g^e - \phi_g^{\Delta r}\|_{l^\infty}$ of the ground state for different Poisson coupling

Table 1: Errors analysis of $\|\phi_g^e - \phi_g^{\Delta r}\|_{l^\infty}$ in ground state versus mesh size Δr for different β .

	$\Delta r = 1/4$	$\Delta r = 1/8$	$\Delta r = 1/16$	$\Delta r = 1/32$
$\beta = -1$	2.306E-04	5.755E-05	1.436E-05	3.563E-06
rate		2.003	2.003	2.011
$\beta = -5$	2.601E-03	6.455E-04	1.614E-04	4.012E-05
rate		2.011	2.000	2.008
$\beta = -10$	7.413E-03	1.827E-03	4.546E-04	1.130E-04
rate		2.021	2.007	2.008
$\beta = -50$	9.300E-02	2.082E-02	5.105E-03	1.264E-03
rate		2.160	2.028	2.014

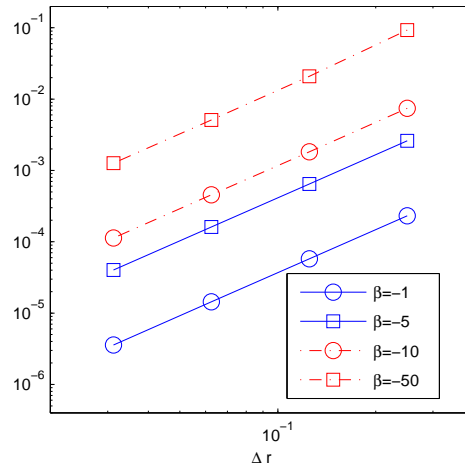


Figure 1: Ground state error versus Δr for different β (source data from Table 1). Straight lines of slope 2 confirm second order convergence in Δr .

constants β . Fig. 1 represent Table 1 by log-log plot of the numerical errors versus Δr . The second order convergence in Δr can be seen clearly by straight lines with a slope 2. Here the convergence rate is defined as $\log_2(\|\phi_g^e - \phi_g^{2\Delta r}\|_{l^\infty} / \|\phi_g^e - \phi_g^{\Delta r}\|_{l^\infty})$.

‘Virial’ identity. A ‘virial’ identity $4\pi E_{kin}(\phi_g) + \beta = 0$ holds and it can be derived by taking derivative of the total energy $E(\phi_g^\lambda)$ with respect to λ where $\phi_g^\lambda = \frac{1}{\lambda}\phi_g(\mathbf{x}/\lambda)$ and $E_{kin}(\phi_g) = \int_{\mathbb{R}^2} |\nabla \phi_g|^2 dx$, we refer to [5] for more details about ‘virial’ identity. Table 2 shows the agreement with the virial identity for ground state between kinetic energy and Poisson constant β . As stated before, the interaction energy E_{int} could be evaluated with relative small domain, numerical results shown in Table 3 confirm it.

Table 2: Virial relations between kinetic energy and β for ground state.

	$\beta = -1$	$\beta = -5$	$\beta = -10$	$\beta = -20$	$\beta = -50$
E_{kin}	7.962E-02	3.979E-01	7.958E-01	1.592	3.979
$\frac{-\beta}{4\pi}$	7.958E-02	3.979E-01	7.958E-01	1.592	3.979

Table 3: Error analysis of Poisson potential ϕ_g^R versus R for $\beta = -5$.

	$R=6$	$R=8$	$R=10$	$R=12$	$R=14$
$\ \phi_g^e - \phi_g^R\ _{l^\infty}$	2.197E-04	1.415E-06	3.437E-09	4.682E-10	< 1.0E-10
$ E_{int}^e - E_{int}^R $	6.838E-04	4.667E-06	1.250E-08	1.500E-09	6.000E-10

Comparisons with BESP. As remarked in Section 1 and [33], homogenous Dirichlet boundary conditions for the Poisson equation on rectangular domain allows a backward

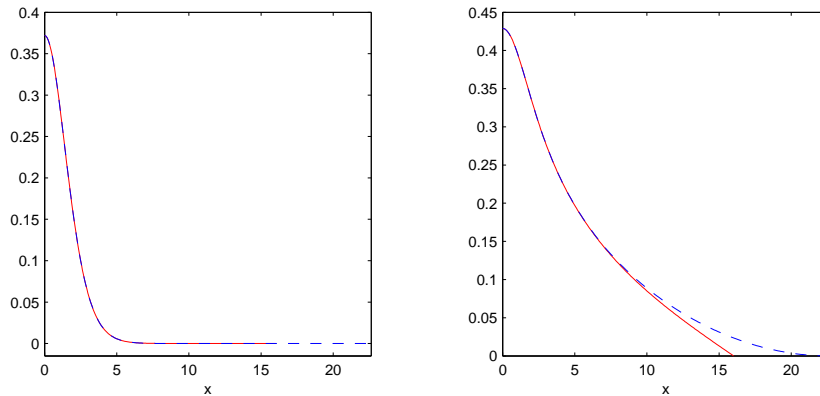


Figure 2: Symmetry property of ground state ϕ_g (left) and Poisson potential φ_g (right) obtained by BEBP.

Euler sine pseudospectral method (BESP) to compute the ground state. However, this homogeneous Dirichlet boundary condition is not proper because the 2D Poisson potential decays algorithmically at far field and simple homogeneous treatment does not respect the algorithmically decay property. For radial symmetric case, e.g., radial symmetric external potential case, ground state obtained by BESP is no longer radial symmetric.

Fig. 2 depicts the ground state $\phi_g(x,y)$ and the Poisson potential $\varphi_g(x,y)$ obtained by BESP for $V = 0$, $\beta = -5$, where the red-solid lines denote $\phi_g(x,0)$ (left), $\varphi_g(x,0)$ (right) and blue-dashed lines denote $\phi_g(\frac{x}{\sqrt{2}}, \frac{x}{\sqrt{2}})$ (left) and $\varphi_g(\frac{x}{\sqrt{2}}, \frac{x}{\sqrt{2}})$ (right). Obviously, the Poisson potential is not radial symmetric, while the ground state ϕ_g appears to be radial symmetric, which could be attributed to the exponentially decay property of ϕ_g .

As we know, the BESP is spectrally accurate for the truncated problem on a rectangular domain with homogeneous Dirichlet boundary conditions, but it does not resolve the 2D SPS spectrally accurate due to the improper treatment of the Poisson potential. Table 4 shows $\|\phi_g^h(\cdot, 0) - \phi_g^e\|_{l^\infty}$ versus mesh size h and $\|\phi_g^L(\cdot, 0) - \phi_g^e\|_{l^\infty}$ versus domain $[-L, L]^2$ where ϕ_g^h is obtained with $L=16$ and ϕ_g^L with uniform mesh size $h=1/16$ by BESP method. The bench mark ϕ_g^e is computed by a finite difference method with $R = 16, \Delta r = 1/1024$. From Table 4, we can conclude that the ground state obtained by BESP is not spectrally accurate to that of 2D SPS and the ground state error $\|\phi_g^L - \phi_g^e\|_{l^\infty}$ decreases to some fixed accuracy as the computation domain increases. Finally, we can conclude that homogeneous Dirichlet boundary condition imposed for the Poisson potential on a rectangular domain does not approximate the 2D Poisson potential, neither does the ground state. One could also expect the same locking phenomenon in the dynamics simulation [3, 33].

Application. We compute the ground states of the 2D SPS with external potential $V = r^2$ for different β . Energies of numerical solutions, obtained by BEFD with $R = 16$, are presented in Table 5. We can see that the total energy $E_{\text{tot}}^\mathcal{S}$, interaction energy $E_{\text{int}}^\mathcal{S}$ and external energy $E_{\text{ext}}^\mathcal{S}(\phi_g) = \int_{\mathbb{R}^2} V \phi_g$ decrease as β decreases, while the kinetic energy $E_{\text{kin}}^\mathcal{S}$ increases.

Table 4: Error analysis of ground state obtained by BESP for $\beta = -5$.

	$h=1$	$h=1/2$	$h=1/4$	$h=1/8$	$h=1/16$
$\ \phi_g^h - \phi_g^e\ _{l^\infty}$	1.668E-05	3.665E-06	4.168E-06	4.303E-06	4.337E-06
	$L=12$	$L=14$	$L=16$	$L=18$	$L=20$
$\ \phi_g^L - \phi_g^e\ _{l^\infty}$	1.102E-05	5.415E-06	4.337E-06	4.336E-06	4.336E-06

Table 5: Energies of ground states for different β with $V=r^2$.

	$\beta = -1$	$\beta = -5$	$\beta = -10$	$\beta = -20$	$\beta = -50$
E_{kin}^g	0.7273	0.8137	0.9341	1.2108	2.2174
E_{int}^g	-0.0103	-0.0746	-0.2051	-0.6187	-2.7538
E_{ext}^g	0.6875	0.6148	0.5362	0.4150	0.2279
E_{tot}^g	1.4045	1.3539	1.2653	1.0071	-0.3085

4.2 Numerical results in computation of the dynamics

To start with, we present accuracy results of SIFD. We choose $R = 16$ and initial value $\psi_0 = e^{-x^2 - (y-2)^2}$ without external potential, i.e., $V = 0$. Let ψ, φ be the ‘exact’ solution computed with very fine mesh size and time step, i.e., $\Delta r = 1/128, \Delta \theta = \pi/128, \tau = 0.0001$ at time $t = 1/2$ and let $\psi^{(\Delta r, \Delta \theta, \Delta t)}, \varphi^{(\Delta r, \Delta \theta, \Delta t)}$ be the numerical solution obtained with mesh size $(\Delta r, \Delta t)$ and time step Δt .

First, we verify the spectral accuracy in the θ -direction by choosing different $\Delta \theta$ with a very small mesh size in the r -direction $\Delta r = 1/128$ and time step $\Delta t = 0.0001$ so that numerical errors coming from r -direction and temporal discretisation can be neglected compared with that from the θ -direction. Table 6 shows errors in θ -direction at time $t = 1/2$ with $\beta = \pm 5$ for wave function ψ and potential φ . Convergence rate here is defined as $\log_2(\|\psi^{(\Delta r, 2\Delta \theta, \Delta t)} - \psi\|_{l^\infty} / \|\psi^{(\Delta r, \Delta \theta, \Delta t)} - \psi\|_{l^\infty})$.

Table 6: Errors of $\|\psi^{(\Delta r, \Delta \theta, \Delta t)} - \psi\|_{l^\infty}$ and $\|\varphi^{(\Delta r, \Delta \theta, \Delta t)} - \varphi\|_{l^\infty}$ (2nd part) in θ -direction.

	$\Delta \theta = \pi/8$	$\Delta \theta = \pi/16$	$\Delta \theta = \pi/32$	$\Delta \theta = \pi/64$
$\beta = -5$	1.451E-02	1.314E-05	3.916E-12	5.624E-14
rate		10.109	21.678	6.122
$\beta = 5$	1.367E-02	3.793E-05	2.899E-11	5.550E-14
rate		8.494	20.319	9.029
$\beta = -5$	4.063E-03	3.047E-07	1.036E-13	1.310E-14
rate		13.703	21.488	2.983
$\beta = 5$	1.671E-03	8.054E-07	9.770E-14	1.055E-14
rate		11.019	22.975	3.211

Table 7: Errors of $\|\psi^{(\Delta r, \Delta \theta, \Delta t)} - \psi\|_{l^\infty}$ and $\|\varphi^{(\Delta r, \Delta \theta, \Delta t)} - \varphi\|_{l^\infty}$ (2nd part) in r -direction.

	$\Delta r = 1/4$	$\Delta r = 1/8$	$\Delta r = 1/16$	$\Delta r = 1/32$
$\beta = -5$	1.024E-02	2.480E-03	6.108E-04	1.491E-04
rate		2.046	2.022	2.034
$\beta = 5$	1.243E-02	3.058E-03	7.491E-04	1.778E-04
rate		2.023	2.029	2.075
$\beta = -5$	3.558E-03	8.805E-04	2.180E-04	5.377E-05
rate		2.015	2.014	2.020
$\beta = 5$	2.638E-03	6.537E-04	1.625E-04	3.981E-05
rate		2.013	2.008	2.029

Table 8: Errors of $\|\psi^{(\Delta r, \Delta \theta, \Delta t)} - \psi\|_{l^\infty}$ and $\|\varphi^{(\Delta r, \Delta \theta, \Delta t)} - \varphi\|_{l^\infty}$ (2nd part) in temporal direction.

	$\tau = 1/128$	$\tau = 1/256$	$\tau = 1/512$	$\tau = 1/1024$
$\beta = -5$	9.600E-05	2.398E-05	5.983E-06	1.484E-06
rate		2.001	2.003	2.011
$\beta = 5$	1.729E-04	4.340E-05	1.086E-05	2.696E-06
rate		1.994	1.999	2.010
$\beta = -5$	2.807E-05	7.024E-06	1.754E-06	4.352E-07
rate		1.999	2.002	2.011
$\beta = 5$	5.486E-05	1.369E-05	3.411E-06	8.457E-07
rate		2.003	2.005	2.012

Next, we test the second order accuracy in the r -direction by choosing different mesh size Δr with a very small mesh size in θ -direction $\Delta \theta = \pi/128$ and time step $\Delta t = 0.0001$ for different Poisson constants. Table 7 shows errors from the r -direction discretisation with $\beta = \pm 5$ for wave function ψ and potential φ , where the convergence rate is defined as $\log_2(\|\psi^{(2\Delta r, \Delta \theta, \Delta t)} - \psi\|_{l^\infty} / \|\psi^{(\Delta r, \Delta \theta, \Delta t)} - \psi\|_{l^\infty})$.

Thirdly, we show the second order accuracy in time by choosing different time step Δt with very small mesh size $(\Delta r, \Delta \theta) = (1/128, \pi/128)$. Table 8 shows errors in time with $\beta = \pm 5$ for wave function ψ and potential φ , where convergence rate is defined as $\log_2(\|\psi^{(\Delta r, \Delta \theta, 2\Delta t)} - \psi\|_{l^\infty} / \|\psi^{(\Delta r, \Delta \theta, \Delta t)} - \psi\|_{l^\infty})$.

From Tables 6-8, we can conclude that SIFD is of spectral accuracy in θ -direction, second-order in r -direction and second-order in time for the wave function ψ and the Poisson potential φ . Fig. 3 shows the second order convergence of the wave function and the Poisson potential in Δr and Δt with $\beta = \pm 5$ (in log-log plot).

We present errors $\|\varphi_R - \varphi\|_{l^\infty}$ and $\|\psi_R - \psi\|_{l^\infty}$ versus different R for $\beta = 5$ in Table 9. From Table 9, we can see that errors $\|\varphi_R - \varphi\|_{l^\infty}$ and $\|\psi_R - \psi\|_{l^\infty}$ decrease as the computation domain increases.

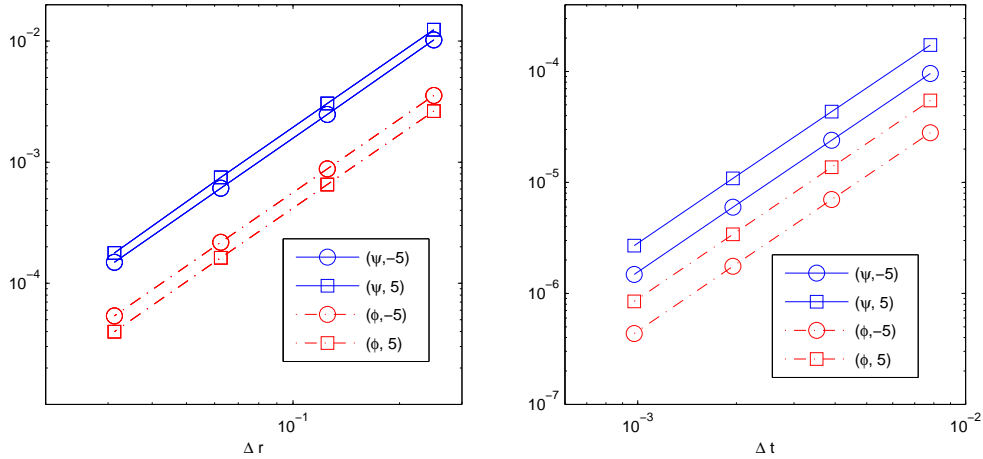


Figure 3: Accuracy diagrams: errors in wave function and Poisson potential for different β (source data from Table 7 (left)-Table 8 (right)). All the straight lines are of slope 2, which confirm the second order convergence in Δr and Δt .

Table 9: Error analysis of $\|\varphi_R - \varphi\|_{l^\infty}$ and $\|\psi_R - \psi\|_{l^\infty}$ versus R with $\beta=5$.

	$R=6$	$R=8$	$R=10$	$R=12$	$R=14$
$\ \psi_R - \psi\ _{l^\infty}$	2.753E-04	3.042E-08	3.356E-09	1.655E-09	7.144E-10
$\ \varphi_R - \varphi\ _{l^\infty}$	1.683E-08	6.462E-09	3.094E-09	1.482E-09	5.701E-10

5 Conclusion

In this paper, we presented a new way of imposing boundary conditions on the 2D Poisson equation when truncating the 2D Schrödinger-Poisson system to a finite domain for computation. By choosing a disc-shaped domain, instead of the more common rectangle-shaped domain with homogeneous Dirichlet boundary conditions, and by using polar coordinates (r, θ) , we derived exact artificial boundary conditions for the Poisson potential, based on truncated Fourier series expansion in θ -direction. We proposed a finite difference scheme on a shifted mesh grid in r -direction to solve ODEs within $\mathcal{O}(MN \log N)$ arithmetic operations where M, N are the number of grid points in r -direction and Fourier bases. A backward Euler and a semi-implicit/leap-frog method were proposed to solve the Schrödinger equation. Combined with the Poisson solver, we implemented our numerical methods to compute the ground state and dynamics of the 2D SPS.

The Poisson potential and the interaction energy can be evaluated accurately by our method. Numerical results confirmed the accuracy and showed the efficiency of our method. Also we made it clear that the backward Euler sine pseudospectral (BESP) method in [33] can not be applied to 2D SPS ground state computation due to improper treatment of the boundary condition for the Poisson equation.

Appendix

Without loss of generality, let us assume $\rho = |\psi|^2$ is radial symmetric and decays exponentially fast, then the Poisson equation φ is also symmetric and satisfies the following equation:

$$\frac{1}{r} \partial_r (r \partial_r \varphi) = -\rho. \quad (\text{A.1})$$

Introduce $\tilde{\varphi} = \sqrt{r} \varphi$ and $\tilde{\psi} = \sqrt{r} \psi$, the Poisson equation is equivalent to

$$\partial_{rr} \tilde{\varphi} + \frac{1}{4r^2} \tilde{\varphi} = -\frac{|\tilde{\psi}|^2}{\sqrt{r}}. \quad (\text{A.2})$$

By a variation of constant coefficient, we have

$$\tilde{\varphi} = C_1(r) \phi_1(r) + C_2(r) \phi_2(r), \quad \phi_1 = \sqrt{r}, \phi_2(r) = \sqrt{r} \ln(r), \quad (\text{A.3})$$

with

$$C_1(r) = \int_0^r \ln(t) |\tilde{\psi}|^2 dt + C_1^0 = \int_0^r \ln(t) |\psi|^2 t dt + C_1^0,$$

$$C_2(r) = -\int_0^r |\tilde{\psi}|^2 dt + C_2^0 = -\int_0^r |\psi|^2 t dt + C_2^0.$$

Then $\varphi = \tilde{\varphi} / \sqrt{r} = C_1(r) + C_2(r) \ln(r)$.

The Poisson potential is finite at $(0,0)$, hence we can deduce $C_2^0 = 0$.

For symmetric density, we have

$$\varphi(\mathbf{0}) = \int_{\mathbb{R}^2} -\frac{1}{2\pi} \ln(|\mathbf{y}|) |\psi|^2(\mathbf{y}) d\mathbf{y} = \int_0^\infty -\ln(t) |\psi|^2 t dt, \quad (\text{A.4})$$

$$\lim_{r \rightarrow 0^+} \varphi(r) = \varphi(0) = \lim_{r \rightarrow 0^+} [C_1(r) + C_2(r) \ln(r)] = C_1^0. \quad (\text{A.5})$$

Up to now, from (A.1) and (A.4) we can rewrite the Poisson potential as

$$\varphi = -\int_r^\infty \ln(t) |\psi|^2 t dt - \left(\int_0^r |\psi|^2 t dt \right) \ln(r). \quad (\text{A.6})$$

By asymptotic analysis in Section 2, we proved that $\varphi(r) \approx a \ln(r) + b$, as $r \rightarrow \infty$. Then we have

$$a = \lim_{r \rightarrow +\infty} \frac{\varphi(r)}{\ln(r)} = -\int_0^\infty |\psi|^2 t dt,$$

$$b = \lim_{r \rightarrow +\infty} [\varphi(r) - a \ln(r)] = 0.$$

In the same way, we can also prove that φ_0 satisfy the same asymptotic analysis, i.e.,

$$\varphi_0 = -\int_r^\infty \ln(t) \rho_0 t dt - \left(\int_0^r \rho_0 t dt \right) \ln(r),$$

$$\varphi_0(r) \approx \left[-\int_0^\infty \rho_0 t dt \right] \ln(r), \quad \text{as } r \rightarrow \infty.$$

Acknowledgments

The second author thanks Prof. Weizhu Bao for suggesting this topic and acknowledges stimulating discussions. Y. Zhang also thanks Prof. Huaiyu Jian for continuous encouragement and support during his Ph.D. research. We also thank the referees for their valuable comments and suggestions to help improve the manuscript. This work was supported by Singapore A*STAR SERC PSF-Grant No. 1321202067 and National Natural Science Foundation of China Grant NSFC41390452 and the Doctoral Programme Foundation of Institution of Higher Education of China as well as by the Austrian Science Foundation (FWF) under grant No. F41 (project VICOM) and grant No. I830 (project LODIQUAS) and grant No. W1245 and the Austrian Ministry of Science and Research via its grant for the WPI.

References

- [1] T. Ando, B. Fowler and F. Stern, Electronic properties of two-dimensional systems, *Rev. Modern Phys.*, 54 (1982), 437-672.
- [2] G. Bastard, *Wave Mechanics Applied to Semiconductor Heterostructure*, Wiley, 1991.
- [3] W. Z. Bao and Y. Y. Cai, Mathematical theory and numerical methods for Bose-Einstein condensation, *Kinet. Relat. Models*, 6 (2013), 1-135.
- [4] W. Z. Bao and Y. Y. Cai, Optimal error estimate of finite difference methods for the Gross-Pitavskii equation with angular momentum rotation, *Math. Comp.*, 82 (2013), 99-128.
- [5] W. Z. Bao, Y. Y. Cai and H. Q. Wang, Efficient numerical methods for computing ground states and dynamics of dipolar Bose-Einstein condensates, *J. Comput. Phys.*, 229 (2010), 7874-7892.
- [6] W. Z. Bao, I-L. Chern and F. Y. Lim, Efficient and spectrally accurate numerical methods for computing ground and first excited states in Bose-Einstein condensates, *J. Comput. Phys.*, 219 (2006), 836-854.
- [7] W. Z. Bao and Q. Du, Computing the ground state solution of Bose-Einstein condensates by a normalized gradient flow, *SIAM J. Sci. Comput.*, 25 (5) (2004), 1674-1697.
- [8] W. Z. Bao, Q. Du and Y. Z. Zhang, Dynamics of rotating Bose-Einstein condensates and its efficient and accurate numerical computation, *SIAM J. Appl. Math.*, 66 (3) (2006), 758-786.
- [9] W. Z. Bao and H. D. Han, High-order local artificial boundary conditions for problems in unbounded domains, *Comput. Methods Appl. Mech. Engrg.*, 188 (2000), 455-471.
- [10] W. Z. Bao, H. Y. Jian, N. J. Norbert and Y. Zhang, Dimension reduction of the Schrödinger equation with Coulomb and anisotropic confining potentials, *SIAM J. Appl. Math.*, 73 (6) (2013), 2100-2123.
- [11] W. Z. Bao, S. Jin and P. A. Markowich, Time-splitting spectral approximations for the Schrödinger equation in the semiclassical regime, *J. Comput. Phys.*, 175 (2002), 487-524.
- [12] W. Z. Bao, N. J. Mauser and H. P. Stimming, Effective one particle quantum dynamics of electrons: A numerical study of the Schrödinger-Poisson- $X\alpha$ model, *Comm. Math. Sci.*, 1 (2003), 809-831.
- [13] C. Bardos, L. Erdős, F. Golse, N. J. Mauser and H.-T. Yau, Derivation of the Schrödinger-Poisson equation from the quantum N -particle Coulomb problem, *C. R. Math. Acad. Sci. Paris*, 334(6) (2002), 515-520.

- [14] C. Bardos, F. Golse and N. J. Mauser, Weak coupling limit of the N -particle Schrödinger equation, *Methods Appl. Anal.*, 7(2) (2000), 275-293.
- [15] N. Ben Abdallah, F. Castella and F. Méhats, Time averaging for the strongly confined nonlinear Schrödinger equation, using almost-periodicity, *J. Differential Equations*, 245 (2008), 154-200.
- [16] H. Chen, Y. Su and B. D. Shizgal, A direct spectral collocation Poisson solver in polar and cylindrical coordinates, *J. Comput. Phys.*, 160 (2000), 453-469.
- [17] X. C. Dong, A short note on simplified pseudospectral methods for computing ground state and dynamics of spherically symmetric Schrödinger-Poisson-Slater system, *J. Comput. Phys.*, 230 (2011), 7917-7922.
- [18] L. Erdős and H.-T. Yau, Derivation of the nonlinear Schrödinger equation from a many body Coulomb system, *Adv. Theor. Math. Phys.*, 5 (2001), 1169-1205.
- [19] F. Ethridge and L. Greengard, A new fast-multipole accelerated Poisson solver in two dimensions, *SIAM J. Sci. Comput.*, 23 (3) (2001), 741-760.
- [20] D. K. Ferry and S. M. Goodnick, *Transport in Nanostructures*, Cambridge University Press, Cambridge, UK, 1997.
- [21] B. Fornberg, A pseudospectral approach for polar and spherical geometries, *SIAM J. Sci. Comput.*, 16 (5) (1995), 1071-1081.
- [22] L. Genovese, T. Deutsch, A. Neelov, S. Goedecker and G. Beylkin, Efficient solution of Poisson equation with free boundary conditions, *J. Comput. Chem.*, 125 074105 (2006).
- [23] L. Greengard and V. Rokhlin, A new version of the fast multipole method for the Laplace equation in three dimensions, *Acta Numerica*, 6 (1997), 229-269.
- [24] H. D. Han and W. Z. Bao, Error estimates for the finite element approximation of problems in unbounded domains, *SIAM J. Numer. Anal.*, 47(4) (2000), 1101-1119.
- [25] H. D. Han and Z. Y. Huang, Exact artificial boundary conditions for the Schrödinger equation in \mathbb{R}^2 , *Commun. Math. Sci.*, 2 (1) (2004), 79-94.
- [26] R. Harrison, I. M. Moroz and K. P. Tod, A numerical study of Schrödinger-Newton equations, *Nonlinearity*, 16 (2003), 101-122.
- [27] M.-C. Lai, W.-W. Lin and W. Wang, A fast spectral/difference method without pole conditions for Poisson-type equations in cylindrical and spherical geometries, *IMA J. Numer. Anal.*, 22 (2002), 537-548.
- [28] M.-C. Lai and W.-C. Wang, Fast direct solvers for Poisson equation on 2D polar and spherical geometries, *Numer. Methods Partial Differential Equations*, 18 (2002), 56-68.
- [29] J. Shen, Efficient spectral-Galerkin methods III: Polar and cylindrical geometries, *SIAM J. Sci. Comput.*, 18 (6) (1997), 1583-1604.
- [30] A. Soba, A finite element method solver for time-dependent and stationary Schrödinger equations with a generic potential, *Commun. Comput. Phys.*, 5 (2009), 914-927.
- [31] I. H. Tan, G. L. Snider, L. D. Chang and E. L. Hu, A self-consistent solution of Schrödinger-Poisson equations using a nonuniform mesh, *J. Appl. Phys.*, 68 (1990), 4071-4076.
- [32] Y. Zhang, Optimal error estimates of compact finite difference discretizations for the Schrödinger-Poisson system, *Commun. Comput. Phys.*, 13 (2013), 1357-1388.
- [33] Y. Zhang and X. C. Dong, On the computation of ground state and dynamics of Schrödinger-Poisson-Slater system, *J. Comput. Phys.*, 230 (2011), 2660-2676.